Optical Review (2023) 30:570–582
https://doi.org/10.1007/s10043-023-00833-9

REGULAR PAPER

A comparative evaluation of 2-D Hilbert transforms and 2-D continuous wavelet transforms for robust phase extraction in complex fringe patterns

Jyoti Singh[1] · Divya Haridas[1] · Anirban Bhowmick[1] · Ramu Pasupathi Sugavaneshwar[1]

Received: 16 March 2023 / Accepted: 20 August 2023 / Published online: 10 September 2023

Abstract
Interferometric techniques are widely used to obtain the real-time phenomena in a majority of applications considering its advantages of non-intrusively, mapping changes in path length as small as the wavelength of the light source used, etc. Interferometers often recorded the changes in the path length in the form of fringe orientation. Depending upon the complexity of the phenomena under observation, interferometric fringes are formed from simple fringe ordinations to complex fringe structures. Extracting phase map from these fringe patterns are highly crucial to evaluate the phase change and the corresponding property change. In order to use the interferometers in its full potential, it is necessary to develop robust and accurate algorithms for phase extraction. In this paper, we discuss 2-D Hilbert transforms (HT) and 2-D continuous wavelet transforms (CWT) techniques to analyze fringe patterns of different orientation and inter-fringe spacing. Simulated interferograms were used to generate implemented fringe patterns with different orientation and spacing. MATLAB software is used to generate these simulated image. In order to check the efficiency of the mentioned algorithm, a white Gaussian filter with different noise levels (0%, 5%, 10%) has been added to the simulated interferograms. Interferometric fringes with noise is a common phenomenon in many transient and turbulent processes. Moreover, the in-build noise in optical configuration and external noises in the testing environment also adds to the noise. Hence, it is necessary to test the accuracy of algorithm for enhanced noises. The results show that the HT algorithm was difficult to implement on complex patterns and was also difficult to implement for a high degree of noise interference. The two-dimensional CWT, on the other hand, has good performance on complex striped patterns and can handle noise disturbances with a good degree of accuracy. The continuous wavelet transform is insensitive to noise interference patterns and gives accurate results. The processing time is very short and it can handle both simple and complex fringe patterns within a very short period of time. It can also be concluded that the 2-D CWT algorithm is very effective and robust.

Keywords Phase extraction · 2-D CWT · Hilbert transform · Simulated images

1 Introduction

Interferometers are often used to determine the morphology of object surfaces especially when the undulations at the surface is in the scale of the wavelength of light. Interferometers generates output as fringe pattern where any change in the fringe pattern can directly correlate to spatial or temporal gradients of the phase field. These fringe pattern captured in the form of gray images using image capturing devices are analyzed to retrieve the gradient in the phase field [1–6]. The phase field then again correlated to a variety of parameters such as refractive index, temperature, and fluid velocity. Two major methods are used for the retrieval of phase from the intensity images

Jyoti Singh and Divya Haridas contributed equally to this work.

✉ Divya Haridas
divyaharidask@gmail.com

Jyoti Singh
jsiphys@gmail.com

Anirban Bhowmick
anirban.bhowmick@outlook.com

Ramu Pasupathi Sugavaneshwar
ramupasupathi.s@vitbhopal.ac.in

[1] VIT Bhopal University, Bhopal, Madhya Pradesh 466114, India

phase-shifting technique [1, 7] and another technique is carrier technique with Fourier transform (FT) [8, 9]. In the phase-shifting technique, each pixel of the fringe pattern is processed. The processing is done separately for each pixel and does not affect the other pixels. Hence, this method gives a better shield for the propagation of errors in the field, which will reduce the cumulative error in the obtained phase field. However, the phase-shifting technique is sensitive to noises, and hence, it is difficult to deal with the complex fringe pattern present in the interferograms. On the other hand, the carrier technique with the FT processes the entire fringe pattern simultaneously. This technique is able to accommodate high-level noises, however, can create an accumulation of errors. Phase determination in a complex fringe or in a closed fringe is tricky, whereas phase determination in an open fringe is much easier because of the presence of the carrier frequency [10]. There are several different transforms from which phase can be determined such as FT, windowed Fourier transform (WFT) [11], and the Hilbert transform (HT) [8, 12, 13], while in closed or complex fringe, it is harder to determine the phase due to the phase ambiguity problem in which there is an absence of carrier frequency [4, 14–17]. In order to solve the phase sign ambiguity problem, a different algorithm has been proposed such as continuous wavelet transform (CWT) [18], regularized phase tracker (RPT) [3, 4, 18–21], and localized Fourier transform (LFT).

The regularized phase tracking algorithm gained attraction in the recent years, where fringe trackers provide a strategy to avoid critical points with a fringe sampling approach [4]. Minimization of the regularized cost function was proposed by Rivera as a method for robust phase demodulation [22]. MarroquinM et.al. proposed another algorithm for the closed-loop fringe pattern, namely the adaptive quadrature filter [23], which is based on Bayesian estimation theory and complex-valued Markov random field prior models. Kemao [24–26] proposed the frequency-guided algorithm to evaluate the local frequencies. The main objective of these techniques is to estimate the phase using the local fringe analysis. Larkin et.al. developed a two-dimensional extension of the HT [14] for fringe demodulation. In addition, the performance of the RPT has also been developed. To improve the computational performance, a new technique for fringe demodulation is based on the analysis of horizontally and vertically oriented fringes [27, 28].

2-D continuous wavelet transform (CWT) [29, 30] algorithm has been commonly used for phase determination. The most common wavelet used is the Morlet and the Gabor wavelet [18]. Phase fringes can naturally be modeled by the 2-D CWT using Gabor atoms (Gabor atoms compose complex periodic functions modulated by Gaussian functions). 2-D CWT will also be used to evaluate the interference fringe pattern with higher noise levels similar to the Hilbert transform methods. Filtering techniques such as windowed Fourier filtering (WFF) or windowed Fourier ridges (WFR) have also been used to further de-noise the retrieved phase field when the interferograms are complex and embrace a high amount of initial noise. The use of filtering in phase wrapped data is depending upon the initial noise level, complexity fringe pattern and effectiveness of the phase wrapping algorithm. The image phase extraction from the wrapped phase has been done using phase unwrapping techniques where the local discontinuity in phase has been removed by the addition or subtraction of 2π [31].

The purpose of this article is to provide a comprehensive overview of phase algorithms employed in fringe projection methods for both basic and complex fringe patterns. Interferograms used in experimental settings with turbulent regimes introduce noise and miscalibration errors in the fringe pattern, making phase determination challenging. Hence, the development of new algorithms becomes crucial to address these challenges. While numerous publications cover a wide range of phase techniques, most focus on traditional methods. However, utilizing computer-generated software allows for the digital construction of diverse fringe patterns. Over the past years, innovative phase-shifting strategies have also been introduced, offering versatile solutions for high accuracy, efficiency, and robust phase retrieval by utilizing various intensity patterns. Modern phase algorithms also incorporate capabilities for absolute phase recovery and temporal phase unwrapping, enabling efficient measurement of complex objects or surfaces. Notably, there is a lack of previous studies summarizing and comparing both these approaches. Consequently, our reviews will focus on these noisy patterns, evaluating various phase techniques while assessing their advantages and drawbacks. Selecting an appropriate phase approach for a specific application requires careful consideration, and this work covers the in-depth study required for the same.

The main objective of this paper is to present some of the recent developments in the 2-D CWT technique for the analysis of optical fringe patterns, which aim to greatly expand the scope of this technique for scientific research and engineering problems. The work aims also to compare the effectiveness of 2-D CWT and 2-D HT techniques in analyzing complex and noisy fringe patterns for direct applications in unsteady state turbulent phenomenon. The present manuscript is organized into the following section: In Sect. 2, the authors presented a brief description of the theory and mathematical modeling of the HT and the 2-D CWT. Sections 3 and 4 are dedicated to the results, discussion and comparison of the above-mentioned algorithms in complex and noisy interferograms.

2 Principles of Hilbert transform and continuous wavelet transform in the fringe pattern processing

The images reproduced using interferometric configurations requires a fair amount post-processing before generating a meaningful conclusion, as the raw images are subjected to background noises. An interferogram gathers errors by different sources as external turbulence, secondary reflections from the surface of the test section, optical components aperture effects, etc. The generation of wrapped and unwrapped phases from these noisy interferograms is a bottleneck problem. A variety of algorithms are used to generate wrapped and unwrapped phases from interferograms. In the following section, we are focusing on 2-D HT and CWT algorithms and compare the effectiveness of the algorithms on complex and noisy interferograms. The next two sections are devoted for the mathematical derivation of the mentioned algorithms.

2.1 Hilbert transform

The principle of the HT is to retrieve the information from phase map signals. In phase maps, it was very complicated to resolve the problem of fringe orientation in vertical and horizontal directions. We incorporate a 2-D discrete HT into the local energy architecture so that image characteristics may be easily spotted. 2-D HT algorithm is used for phase information. 2-D HT offers high accuracy in signal or phase reconstruction. It contains the complete information about the optical field investigation, including the uniform distribution of the phase lines, the phase singularities and the saddle points of the intensity of the color fringes. The analytical and the complex signal *V(x,y)* can be expressed as

$$V(x,y) = f(x,y) + i\hat{f}(x,y) \tag{1}$$

where x and y are the coordinates of the fringe pattern. *f(x,y)* represents as the intensity of the optical fringes. Here, i refers to the imaginary part of the function.

The 2-D HT of the complex interferograms can be introduced as

$$\hat{f}(x,y) = f(x,y) * h(x,y) \tag{2}$$

(*) represents the convolution operator, and $\hat{f}(x,y)$ is the initial signal of the 2-D Hilbert transform.

$$h(x,y) = \begin{cases} 1, 0 \le x \le \frac{n}{2}, 0 \le y \le \frac{n}{2} \\ 0, \text{ elsewhere} \end{cases} \tag{3}$$

Here, n represents the image dimensions in the x and y directions. The phase distribution of the simulated interferograms can be expressed as

$$\phi(x,y) = \tan^{-1}\frac{\text{Imag}(V(x,y))}{\text{Real}(V(x,y))} \tag{4}$$

where $\phi(x,y)$ is the phase distribution of the images.The 2-D HT refers to the implementation of the Fast Fourier Transform (FFT). Phase shifting technique is used in HT with $\pm 90°$.

2.2 Governing equation of the 2-D continuous wavelet transform for the different pattern of the fringe analysis

In image processing, the wavelet transform has become a very vital tool in the various fields such as in physics, applied mathematics, and engineering. Using 2-D CWT, it is possible to obtain detailed shift-invariant spectral information of different locations and orientations of the analyzed dataset over a continuous domain of the analyzed data. Image analysis and features detection in 2-D CWT are carried out with particular attention to the detection of singularities (contours and sharp transitions).

Mathematically, images can be expressed as in the terms of the intensity are

$$I(x,y) = e^{i\phi(x,y)} = \cos\phi(x,y) + i\sin\phi(x,y) \tag{5}$$

Mathematically, the two-dimensional continuous wavelet transform for a different fringe pattern can be expressed as

$$\text{CWT}(\xi,\eta,\theta,a) = \int_{-\infty}^{\infty}\int_{-\infty}^{\infty} I(x,y)\psi^{*}_{\xi,\eta,\theta,a}(x,y)dxdy \tag{6}$$

Here,$\psi_{\xi,\eta,\theta,a}\,(x,\,y)$ represents the wavelet family, *(x,y)* are the image coordinates in the 2×2 dimensions and θ in the range of $[-\pi,\pi]$.

Family wavelets are scaled by factor a, shifted by ξ and η and oriented by angle θ. Complex conjugates are denoted by symbol *.

In 2-D, Gabor wavelet can be expressed as

$$\psi_{\xi,\eta,\theta,a}(x,y) = \exp\left[-\frac{\pi\left[(x-\xi)^2 + (y-\eta)^2\right]}{a}\right] \times \exp\left[i2\pi\frac{f}{a}[(x-\xi)\cos\theta + (y-\eta)\sin\theta]\right] \tag{7}$$

Here, f is the frequency. Putting the values of Eqs. (5) and (7) in Eq. (6), we get

$$\mathrm{CWT}(\xi,\eta,\theta,a)=\int_{-\infty}^{\infty}\int_{-\infty}^{\infty}\exp[i\phi(x,y)]\times\exp\left[-\frac{\pi\left[(x-\xi)^2+(y-\eta)^2\right]}{a}\right]\times\exp\left[-i2\pi\frac{f}{a}[(x-\xi)\cos\theta+(y-\eta)\sin\theta]\right]dxdy \tag{8}$$

Simplifying Eq. (7), let us assume $x'=x-\xi, y'=y-\eta$ and $(\chi,\gamma)=(\frac{f}{a}cos\theta,\frac{f}{a}sin\theta)$, where (χ,γ) are the frequency vector which is being in the direction of θ. Solving Eq. (7), using Taylor's expression, we found that

$$\phi\left(x'+\xi,y'+\eta\right)\approx\phi(\xi,\eta)+\left[\frac{\partial\phi}{\partial\xi}x'+\frac{\partial\phi}{\partial\eta}y'\right] \tag{9}$$

Then, we can approximate Eq. (7) as follows:

$$\mathrm{CWT}(\xi,\eta,\theta,a)\approx\exp[i\phi(\xi,\eta)]\int_{-\infty}^{\infty}\int_{-\infty}^{\infty}\exp\left\{i\left[\frac{\partial\phi}{\partial\xi}x'+\frac{\partial\phi}{\partial\eta}y'\right]\right\}\times\exp\left[-\pi\frac{\left(x'^2+y'^2\right)}{a}\right]\times\exp\left[-i2\pi\left(\chi x',\gamma y'\right)\right]dx'dy' \tag{10}$$

A scaled Gaussian function modulating a 2-D complex periodic function with frequency $\nabla\psi(\xi,\eta)/2\pi$ is represented by the integral as the Fourier transform of the function. Therefore, using Fourier theorems, we find the following:

$$\mathrm{CWT}(\xi,\eta,\theta,a)\approx\exp[i\phi(\xi,\eta)]\times\exp\left\{-a\pi\left[\left(\chi-\frac{1}{2\pi}\frac{\partial\phi}{\partial\xi}\right)^2+\left(\gamma-\frac{1}{2\pi}\frac{\partial\phi}{\partial\eta}\right)^2\right]\right\} \tag{11}$$

It can be argued that 2-D CWT based on Gabor atoms provides a local spectral energy density concentrated around a given position in the frequency domain, which is adequate for modeling phase images. The 2-D CWT is remarkable for its detailed frequency and oriented decomposition of *I(x,y)*. The orientation of the angle θ lies in the range of $[-\pi,\pi]$.

2.3 Principles of windowed Fourier transform method

In our current work, which is included in the study, the WFT approach is applied to provide findings with superior phase map quality. The first method for dealing with WFT is the substitution of a wrapped phase image into an exponential phase field, which is represented as

$$f(x,y)=b(x,y)e^{j(\Delta\phi(x,y))} \tag{12}$$

Here,*b(x,y)* is the amplitude which is kept constant, i.e., equal to 1.

The 2-D WFT and 2-D inverse WFT are commonly represented as

$$Sf(u,v,\xi,\eta)=\int_{-\infty}^{\infty}\int_{-\infty}^{\infty}f(x,y)g(x-u,y-v)\exp(-j\xi x-j\eta y)\mathrm{d}x\,\mathrm{d}y \tag{13}$$

$$f(x,y)=\frac{1}{4\pi^2}\int_{-\infty}^{\infty}\int_{-\infty}^{\infty}\int_{-\infty}^{\infty}\int_{-\infty}^{\infty}Sf(u,v,\xi,\eta)g(x-u,y-v)\times\exp(j\xi x+j\eta y)\mathrm{d}\xi\mathrm{d}\eta\mathrm{d}u\,\mathrm{d}v \tag{14}$$

Here, j represents the imaginary component which is equal to $\sqrt{(-1)}$ and *g(x-u,y-v)* denotes to the length of the WFT a finite spatial extension. The window function *g(x,y)* is the normalized Gaussian function which is indicated with the following equation:

$$g(x,y)=\frac{1}{\sqrt{\pi\sigma_x\sigma_y}}\exp\left(-\frac{x^2}{2\sigma_x^2}-\frac{y^2}{2\sigma_y^2}\right) \tag{15}$$

Here, σ_x and σ_y are used to analyze the standard distribution of Gaussian function traveling in the x and y directions respectively.

The windowed Fourier transform method is initially applied to the original image and after applying its power spectrum $|Sf(u,v,\xi,\eta)|$ is estimated. The filter function $|H(u,v,\xi,\eta)|$ is expressed in this method which is taken as

$$H(u,v,\xi,\eta)=\begin{cases}Sf(u,v,\xi,\eta) & \text{if } |Sf(u,v,\xi,\eta)|\geqslant thr\\ 0 & \text{if } |Sf(u,v,\xi,\eta)|\leqslant thr\end{cases} \tag{16}$$

Here, *thr* represents the threshold value. After getting the filtered results of WFF, phase unwrapping must be done to make the continuous phase map. Quality Guided algorithm has been taken for phase unwrapping to deal with the noisy interferograms. The WFF depends on nine various parameters which include the window size along the x direction and the y direction, i.e., taken as 10 throughout our work. It includes the low bound and high bound of frequency ξ_l and ξ_h in x direction and the increasing value of ξ_i. Similarly, in the y direction, the high bound η_h and low bound η_l of frequency has been taken and the increasing value of η_i. The threshold value, *thr* has also been considered which is set as 6 in this work.

3 Fringe analysis in simulated interferograms using 2-D HT and CWT

The interferometric images are produced with different fringe orientation by simulating the fringe orientation mathematically. Six different fringe orientations are simulated interferograms and all the simulated images were processed

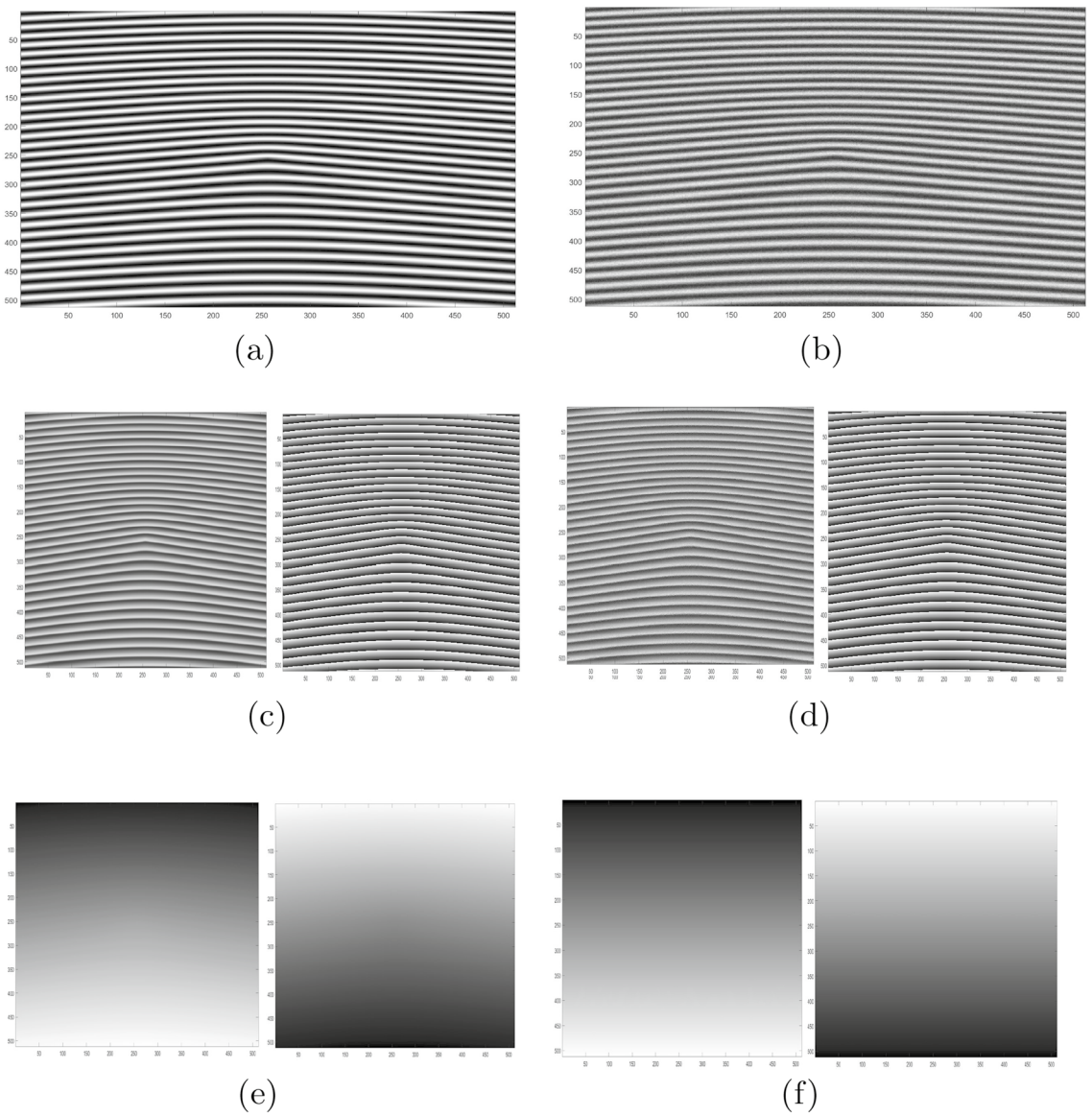

Fig. 1 Simulated fringe patterns in vertical fringe orientation. (**a**) Original image. (**b**) Noisy image (10%). (**c**) Wrapped phase corresponds to image (**a**). (**d**) Wrapped phase corresponds to image (**b**). (**e**) Unwrapped phase map corresponds to image (**c**) and (**f**) Unwrapped phase map corresponds to image (**d**)

using MATLAB software with a computer equipped with a 2.4 GHz Core i5. The results obtained using the simulated images has been evaluated to identify the effectiveness and the accuracy of 2-D CWT and the 2-D HT. The effectiveness of the image processing techniques has been evaluated for higher degree of noises which is a frequent problem in transient and turbulent phenomena. A white Gaussian noise has been added on the simulated interferograms with different percentage levels (0%,5%,10%). The dimensions of all simulated images are set as 512×512 pixels for uniformity.

Figure 1 shows the simulated images and the results obtained using 2-D HT and CWT for the first fringe configuration (vertical parallel fringes). The computer-simulated images of Fig. 1 have been carried out by the following governing equation. In this study, computer-generated items with a fringe pattern of 512×512 pixels value will be employed for testing purposes [32]:

$$\begin{aligned}\phi(x,y) =& 3\times(1-x)^2\times\exp\left(-\left(x^2\right)-(y+1)^2\right)\\ &-10\times\left(x/5-x^3-y^5\right)\times\exp\left(-x^2-y^2\right)\\ &-1/3\times\exp\left(-(x+1)^2-y^2\right)\end{aligned}\tag{17}$$

The intensity of the fringe pattern can be expressed as

$$I(x,y) = 0.3 \times \phi(x,y) + cos(2\pi \times 0.06x + \phi(x,y)) + noise \quad 1 \leqslant x, y \leqslant 512 \tag{18}$$

Figure 1(a) represents the interferogram with lowest level of noise (0%) and Fig. 1(b) shows the image with highest amount of noise (i.e., 10%). Figure 1(c) and (d) shows the wrapped phase map of Fig. 1(a) and (b) respectively, extracted using the aforementioned phase extraction algorithm. White Gaussian filter is applied before wrapping the phase. The wrapped phases are unwrapped using Quality Guided Algorithm [11]. The unwrapped images are shown in Fig. 1(e) and (f) respectively.

Figure 1a shows vertical fringe orientation simulated using MATLAB. A similar pattern of nomenclature is followed as that of Fig. 1(a–f) in order to present the wrapped and unwrapped phases of vertical fringe orientation with different noise levels. The governing equation of Fig. 2 which has been generated by the MATLAB software can be expressed as follows:

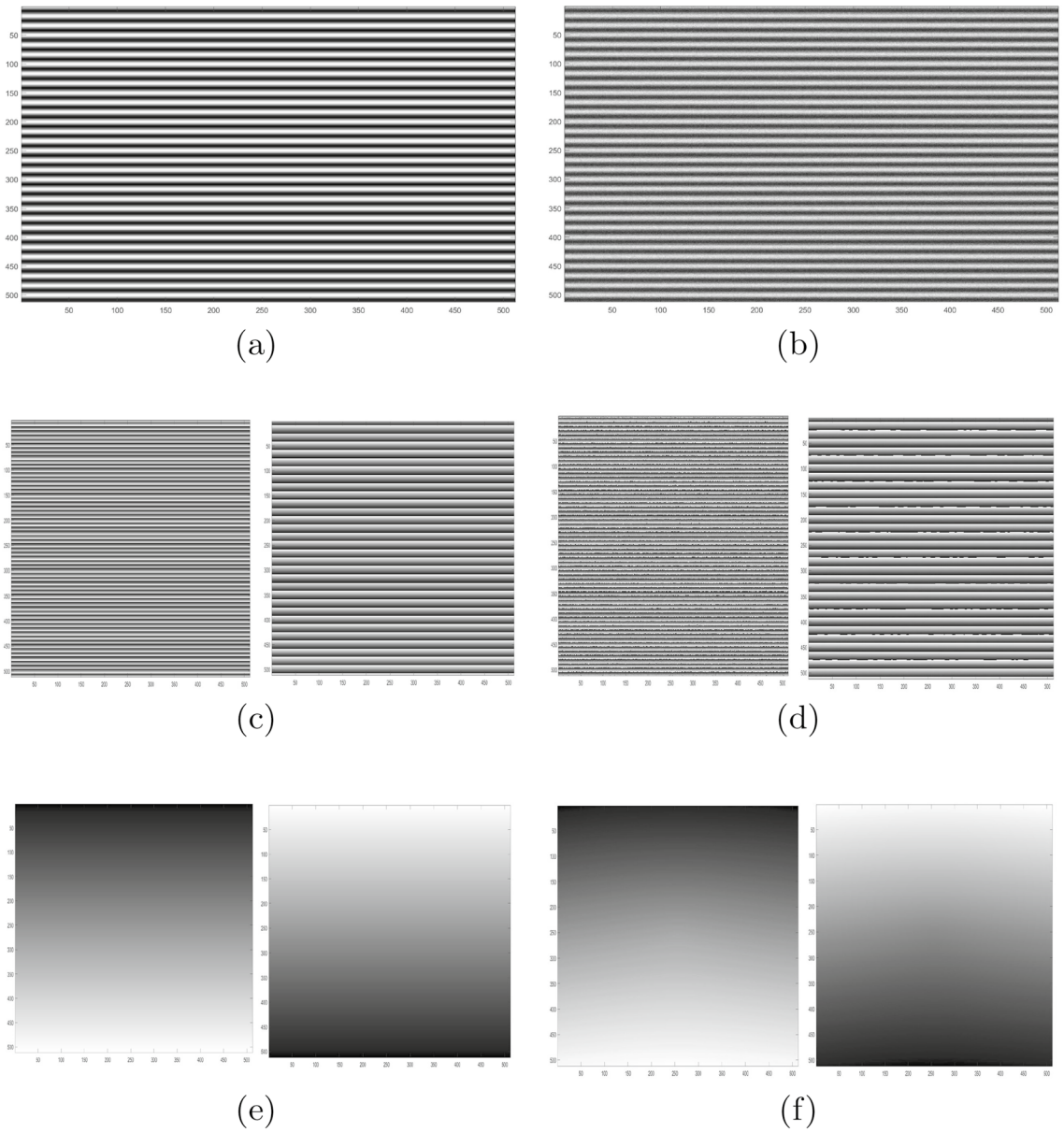

Fig. 2 Simulated fringe patterns in horizontal fringe orientation. (**a**) Original image. (**b**) Noisy image (10%). (**c**) Wrapped phase corresponds to the image (**a**). (**d**) Wrapped phase corresponds to image (**b**). (**e**) Unwrapped phase map corresponds to image (**c**) and (**f**). Unwrapped phase map corresponds to image (**d**)

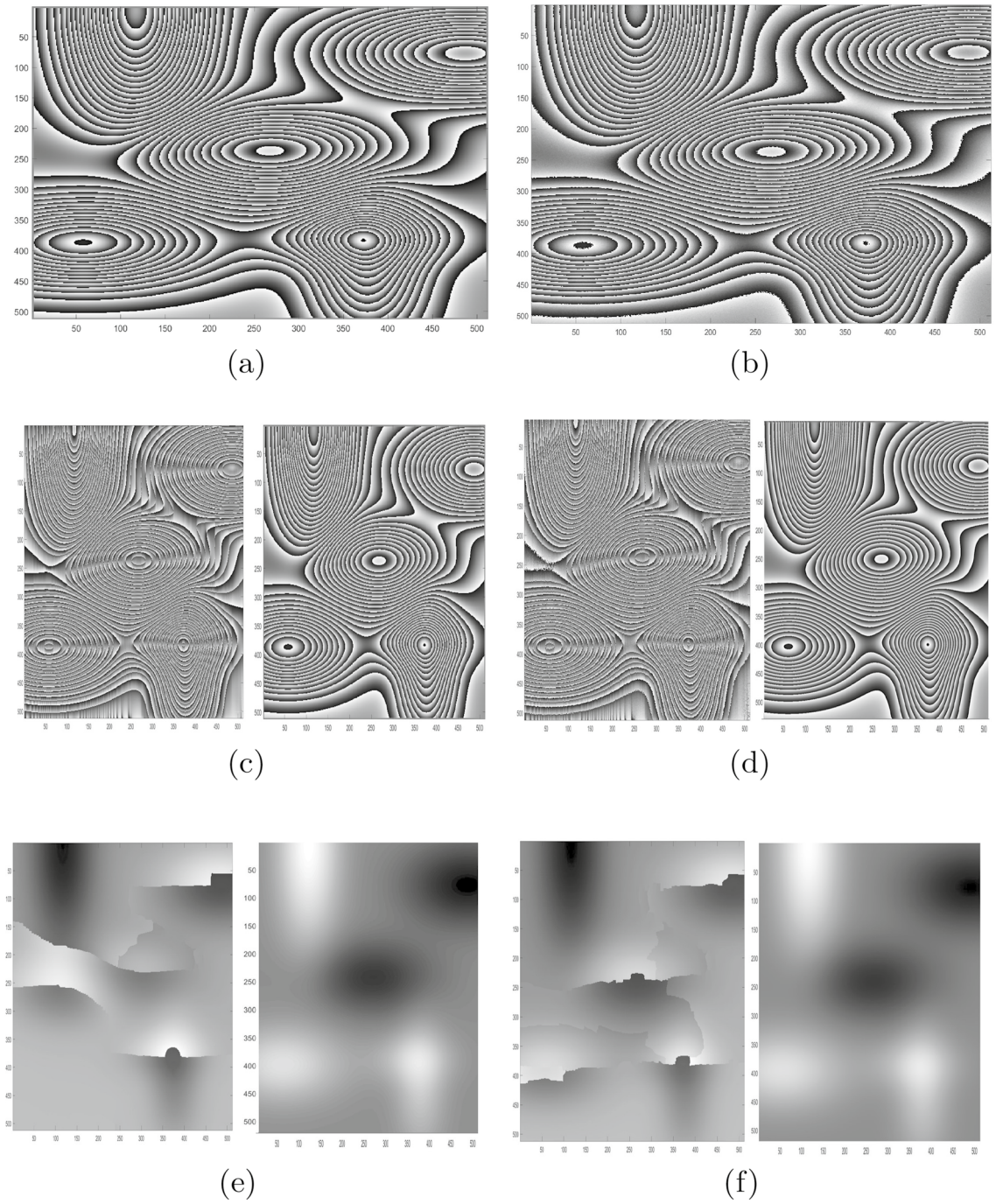

Fig. 3 Simulated fringe in complex fringe pattern-1. **a** Original image. **b** Noisy image (10%). **c** Wrapped phase corresponds to image (**a**). **d** Wrapped phase corresponds to image (**b**). **e** Unwrapped phase map corresponds to image (**c**) and **f**. Unwrapped phase map corresponds to image (**d**)

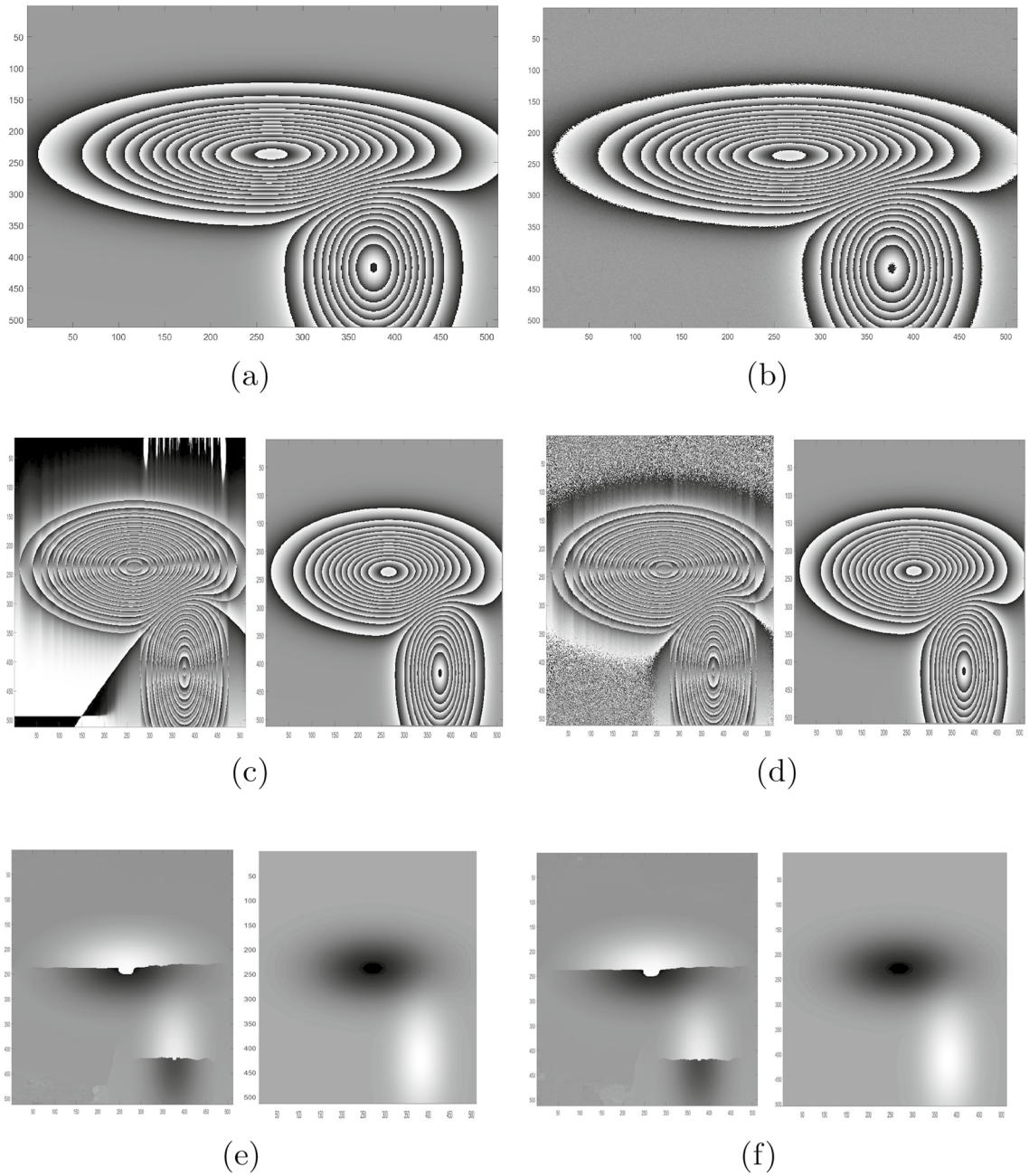

Fig. 4 Simulated fringes in complex fringe pattern-2. **a** Original image. **b** Noisy image (10%). **c** Wrapped phase corresponds to image (**a**). **d** Wrapped phase corresponds to image (**b**). **e** Unwrapped phase map corresponds to image (**c**) and **f**. Unwrapped phase map corresponds to image (**d**)

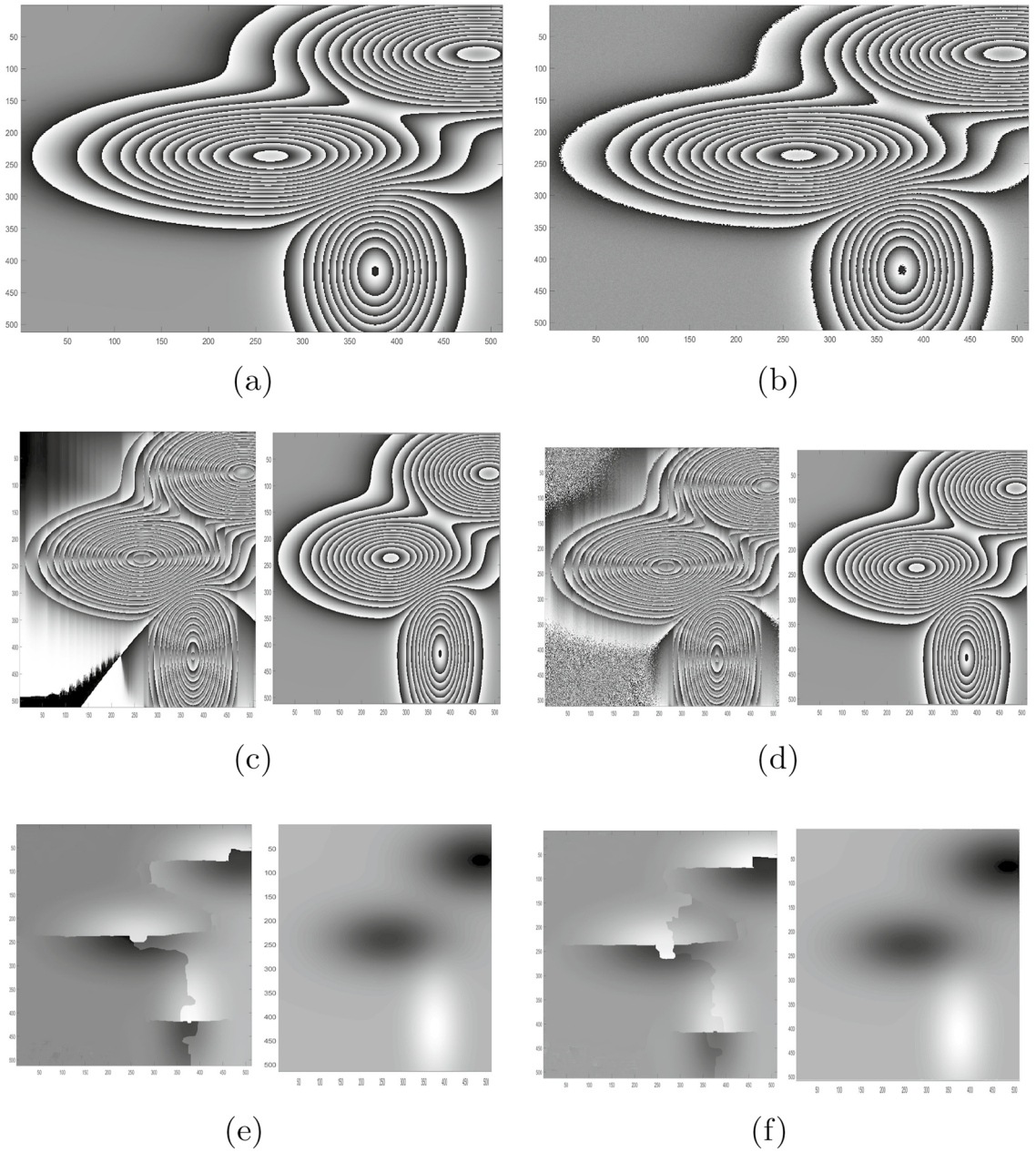

Fig. 5 Simulated fringes in complex fringe pattern-3. **a** Original image. **b** Noisy image (10%). **c** Wrapped phase corresponds to image (**a**). **d** Wrapped phase corresponds to image (**b**). **e** Unwrapped phase map corresponds to image (**c**) and **f**. Unwrapped phase map corresponds to image (**d**)

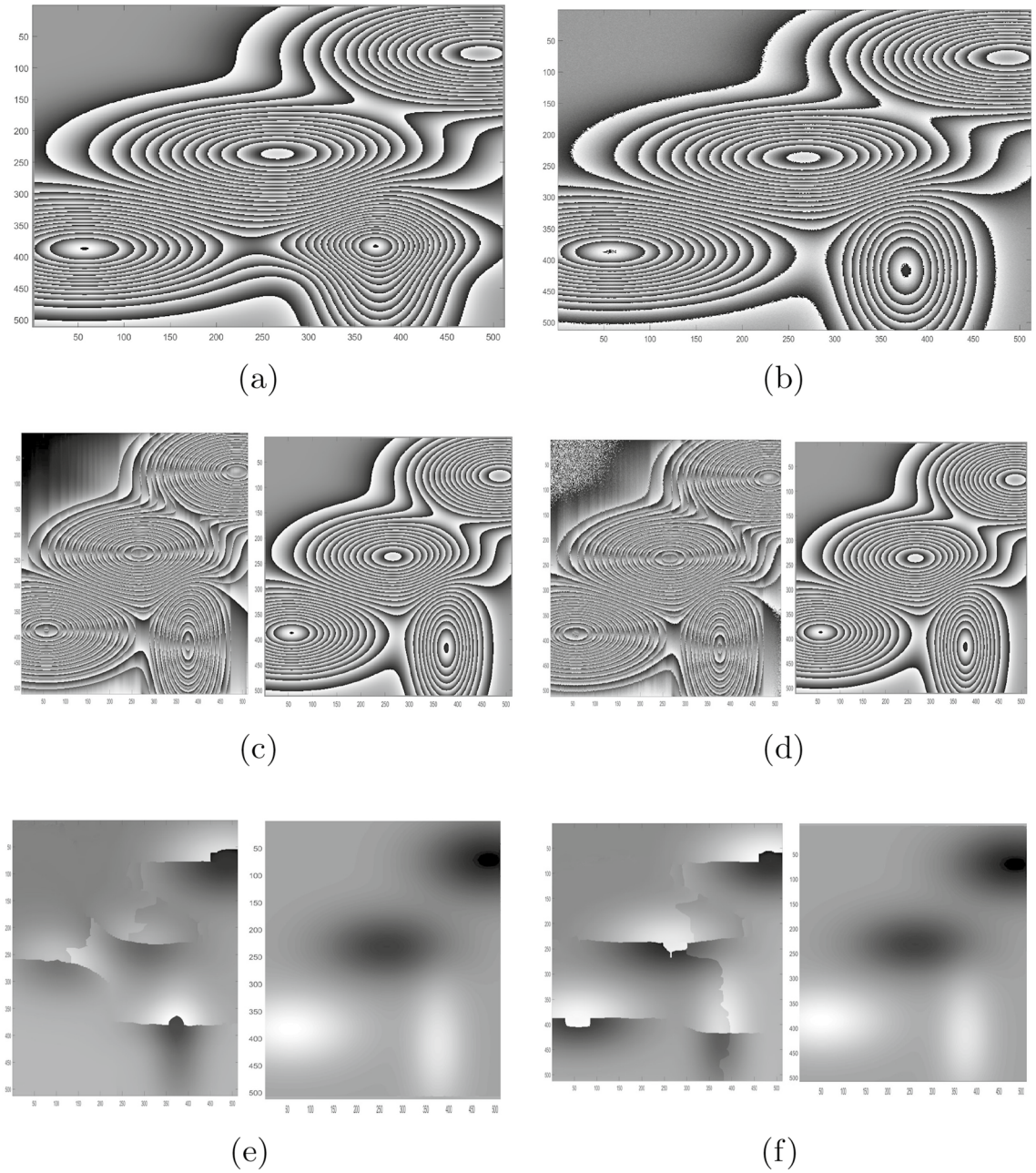

Fig. 6 Simulated fringe in complex fringe pattern-4. **a** Original image. **b** Noisy image (10%). **c** Wrapped phase corresponds to image (**a**). **d** Wrapped phase corresponds to image (**b**). **e** Unwrapped phase map corresponds to image (**c**) and **f**. Unwrapped phase map corresponds to image (**d**)

$$\phi(x,y) = 0.05 \times sqrt((x-256)^2 + (y-256)^2) \tag{19}$$

The background fringe pattern can be expressed as

$$I(x,y) = cos(2\pi x \times 0.06) - \phi(x,y) + 1.5 + noise \quad 1 \leqslant x,y \leqslant 512 \tag{20}$$

The respective images (a) in the figures from Figs. 3, 4, 5, and 6 are the another computer-generated simulated interferograms with different noise levels and having a size of 512×512 pixels. The phase value of a simulated fringe pattern can be developed by the following equation:

$$\begin{aligned}
\phi(x,y) &= 60 \times \exp\left[-\frac{(x-120)^2}{2\times(40)^2} + \frac{(y-160)^2}{2\times(80)^2}\right] \\
\phi(x,y) &= \phi(x,y) - 80 \times \exp\left[-\frac{(x-10)^2}{2\times(100)^2} + \frac{(y+20)^2}{2\times(45)^2}\right] \\
\phi(x,y) &= \phi(x,y) + 120 \times \exp\left[-\frac{(x+140)^2}{2\times(50)^2} + \frac{(y+250)^2}{2\times(120)^2}\right] \\
\phi(x,y) &= \phi(x,y) + 45 \times \exp\left[-\frac{(x-100)^2}{2\times(70)^2} + \frac{(y-120)^2}{2\times(30)^2}\right] \\
\phi(x,y) &= \phi(x,y) + 85 \times \exp\left[-\frac{(x+120)^2}{2\times(95)^2} + \frac{(y-130)^2}{2\times(45)^2}\right] \\
\phi(x,y) &= \phi(x,y) - 100 \times \exp\left[-\frac{(x-230)^2}{2\times(10)^2} + \frac{(y+180)^2}{2\times(50)^2}\right]
\end{aligned} \tag{21}$$

The intensity of all the simulated fringe pattern can be given by

$$I(x,y) = atan\left[\frac{sin\phi(x,y)}{cos\phi(x,y)}\right] + noise \quad 1 \leqslant x,y \leqslant 512 \tag{22}$$

The detailed equations for Figs. 4, 5, and 6 are provided in the Appendix section of the paper for further reference.

Figures 3a, 4a, 5a, and 6a represent the simulated interferograms with enclosed and complex fringe orientation with 0% noise and Figs. 3b, 4b, 5b, and 6b represent the corresponding interferograms at 10% noise. There is some major difference in complex interferograms represented in Figs. 3, 4, 5, and 6 as compared to Figs. 1 and 2. In complex interferograms the fringe variations are not restricted to a single direction, the fringe gradient is spread in multiple dimensions. Moreover, the distance between the adjusted fringes is not uniform, there are multiple points where the fringe density is higher as compared to the other points. Figures 3c, d, 4c, d, 5c, d, and 6(c)–(d) represent the phase wrapped images of the simulated images with 2-D HT and 2-D CWT. Figures 3e, f, 4e, f, 5e, f, and 6e, f are the unwrapped images of the corresponding wrapped phase images. It is to be noted that in each unwrapped phase image is obtained after filtering the image with the windowed Fourier filtering (WFF)

Table 1 RMSE, NMSE and processing time of the 2-D Hilbert transform and 2-D CWT at different noise levels for images in Figs. 1 and 2

Figures	Noise (%)	Processing time (seconds) Hilbert 2-D CWT	RMSE Hilbert 2-D CWT	NMSE Hilbert 2-D CWT
Figure 1	0	16.92 13.74	1.733 0.76	5.0918e-06 1.11e-04
	5	17.03 13.79	1.734 0.763	5.0955e-06 1.10e-04
	10	17.11 13.88	1.735 0.764	5.10e-06 1.0e-04
Figure 2	0	15.97 14.11	1.1488 0.8145	0.1310 2.29e-04
	5	16.14 14.15	1.1493 0.8147	0.1311 2.28e-04
	10	16.209 14.16	1.1496 0.8148	0.1312 2.27e-04

Table 2 RMSE, NMSE and processing time of the 2-D Hilbert transform and 2-D CWT at different noise levels in complex fringe orientations (Figs. 3, 4, 5, 6)

Figures	Noise (%)	Processing time (seconds) Hilbert 2-D CWT	RMSE Hilbert 2-D CWT	NMSE Hilbert 2-D CWT
Figure 3	0	67.58 11.28	1.9968 1.3	0.0098 2.7673e-04
	5	68.97 11.32	1.9916 1.3355	0.0098 2.7674e-04
	10	69.97 11.35	1.9876 1.344	0.0097 2.7676e-04
Figure 4	0	69.44 10.72	1.781 1.21	0.0019 2.5364e-04
	5	69.98 10.75	1.7238 1.2050	0.0018 2.5362e-04
	10	70.00 10.71	1.7006 1.2048	0.0017 2.5360e-04
Figure 5	0	69.29 11.35	1.8424 1.2478	0.0036 6.4820e-05
	5	69.31 11.37	1.8118 1.2472	0.0035 6.4822e-05
	10	69.49 11.40	1.8002 1.2470	0.0034 6.4824e-05
Figure 6	0	69.11 11.4	1.944 1.29	0.3022 0.0067
	5	69.25 11.46	1.9391 1.2905	0.3006 0.0065
	10	69.56 11.593	1.9360 1.2902	0.2994 0.0063

algorithm. The filtering algorithm is kept uniform for all types of fringes for better comparison.

The comparison was made of the performance of 2-D HT and 2-D CWT in vertical, horizontal, and complex fringe patterns. The performance of HT and CWT is almost comparable in the case of vertical and horizontal fringe interferograms whereas 2-D CWT gives better performance in wrapped fringes as compared to 2-D HT in case of complex and closed fringes. The phase wrapping is tricky in HT in these images due to lack in carrier frequency. It is also found from the images that in case of fringes contaminated with higher degree of noises, both techniques failed to give satisfactory results in wrapped phases and the wrapped phase has ended up with significant amount of error. The errors in the wrapped phase in turn propagate into the unwrapped phases and hence the evaluation of the subsequent quantities. In order to place the above comparison drawn qualitatively from the wrapped images, the authors evaluated the root mean square error in each case, which is an effort to quantitatively put forth the effectiveness of each technique in different fringe orientation.

The root mean square error (RMSE) is being defined as follows:

$$\epsilon = \sqrt{\sum |\emptyset - \emptyset'|^2} \tag{23}$$

Here, $\emptyset$ denotes the noiseless phase map and $\emptyset'$ represents the wrapped phase map, respectively.

To evaluate the phase discrepancies error, we have evaluated normalized mean square error.

The normalized mean square error (NMSE) can be calculated by the following equation:

$$\in = \frac{\sum_{|\phi-\phi'|^2}}{\sum_{|\phi|^2}}$$

where ϕ and ϕ' are the noiseless and estimated wrapped phase map, respectively.

Tables 1 and 2 illustrate the processing/computational time, root mean squared error (RMSE), and normalized mean square error (NMSE) of the different algorithms employed in the study. It can be observed that the time employed for 2-D HT is more as compared to 2-D CWT irrespective of the orientation of fringes. Comparing the RMSE and NMSE values in Tables 1 and 2, it is observed that the phase discrepancies obtained in Hilbert are more as compared to CWT. It is also found that the CWT provides better accuracy with better computational efficiency.

4 Discussion and conclusion

The conclusion drawn from the literature is that different image processing algorithms are used for phase wrapping the images for further processing. These algorithms often encounter a variety of drawbacks such as: (a) sometimes previous computational results are used, so the software must be updated before another simulated pattern can be used. (b) Implementation is difficult. (c) The processing time for the highest noise levels is high. (d) Sometimes the performance for the highest noise levels is lower. (e) Multiple trials are required to obtain accurate results. (f) The smoothing of the phase (phase envelope) is made difficult by the enveloped phase.

The manuscript compares the performance of 2-D Hilbert transform and 2-D continuous wavelet transform to decode the phase values from different fringe orientations which we normally encounter with different path length-depended phenomena. Six different fringe orientations are considered to incorporate a wide range of fringe orientation and spacing. The results of the phase wrapping algorithms are evaluated in terms of computational speed, NMSE and RMSE values. The results evaluated in terms of qualitative and quantitative analyses show that the 2-D wavelet transform exhibits improved processing speed and high accuracy in comparison with Hilbert transform for all fringe orientation discussed. Hence, it can be concluded that 2-D CWT is more robust as compared to Hilbert transform algorithm with better processing speed.

Supplementary Information The online version contains supplementary material available at https://doi.org/10.1007/s10043-023-00833-9.

Availability of data and materials The dataset generated during and/or analyzed during the current study are available from the corresponding author on reasonable request.

Code availability The code is available on reasonable request.

Declarations

Conflict of interest The authors have no conflicts of interest to declare that are relevant to the content of this article.

Ethical approval Not required.

Consent to participate Yes.

Consent for publication Yes.

References

1. Robinson, D.W., Reid, G.T., De Groot, P.: Interferogram analysis: digital fringe pattern measurement techniques. Phys. Today **47**(8), 66 (1994)
2. Huntley, J.M.: Automated fringe pattern analysis in experimental mechanics: a review. J. Strain Anal. Eng. Des. **33**(2), 105–125 (1998)
3. Dorrío, B., Fernández, J.: Phase-evaluation methods in whole-field optical measurement techniques. Meas. Sci. Technol. **10**(3), 33 (1999)
4. Servin, M., Marroquin, J., Cuevas, F.: Fringe-follower regularized phase tracker for demodulation of closed-fringe interferograms. JOSA A **18**(3), 689–695 (2001)
5. Pérez, A.M., Rodríguez-Zurita, G., Flores-Muñoz, V., Parra-Escamilla, G., Serrano-García, D., Martínez-García, A., Islas-Islas, J., Ortega-Mendoza, J., Lechuga, L.G., Toto-Arellano, N.-I.: Dynamic Mach-Zehnder interferometer based on a Michelson configuration and a cube beam splitter system. Opt. Rev. **26**, 231–240 (2019)
6. Yu, X., Zuo, S., Zhang, Y., Ma, Y., Wang, R., Yang, W., Tian, K., Geng, T., Wang, P.: A Mach-Zehnder interferometer based on peanut structure for temperature and refractive index measurement. Opt. Rev. **29**(6), 492–497 (2022)
7. Creath, K.: Phase measurement interferometry techniques. Prog. Opt. **26**, 348–393 (1988)
8. Haridas, D., Srivastava, A., et al.: Interferometric study of nanofluid-based heat transfer phenomena in compact channels. Int. J. Therm. Sci. **96**, 70–84 (2015)
9. Takeda, M., Ina, H., Kobayashi, S.: Fourier-transform method of fringe-pattern analysis for computer-based topography and interferometry. JOSA **72**(1), 156–160 (1982)
10. Malacara, D., Servin, M., Malacara, Z.: Interferogram analysis for optical testing. Opt. Eng. **84**, 568 (2018)
11. Kemao, Q.: Two-dimensional windowed Fourier transform for fringe pattern analysis: principles, applications and implementations. Opt. Lasers Eng. **45**(2), 304–317 (2007)
12. Trusiak, M., Patorski, K., Wielgus, M.: Hilbert-Huang processing and analysis of complex fringe patterns. Interferometry XVII **9203**, 148–162 (2014)
13. Zenkova, C.Y., Gorsky, M., Ryabyj, P.: Phase retrieval of speckle fields based on 2D Hilbert transform. Opt. Mem. Neural Netw. **24**(4), 303–308 (2015)
14. Larkin, K.G.: Natural demodulation of two-dimensional fringe patterns II stationary phase analysis of the spiral phase quadrature transform. JOSA A **18**(8), 1871–1881 (2001)
15. Quan, C., Tay, C.J., Yang, F., He, X.: Phase extraction from a single fringe pattern based on guidance of an extreme map. Appl. Opt. **44**(23), 4814–4821 (2005)
16. Tian, C., Yang, Y., Liu, D., Luo, Y., Zhuo, Y.: Demodulation of a single complex fringe interferogram with a path-independent regularized phase-tracking technique. Appl. Opt. **49**(2), 170–179 (2010)
17. Kai, L., Kemao, Q.: Improved generalized regularized phase tracker for demodulation of a single fringe pattern. Opt. Express **21**(20), 24385–24397 (2013)
18. Escalante, N., Villa, J., de la Rosa, I., de la Rosa, E., González-Ramírez, E., Gutiérrez, O., Olvera, C., Araiza, M.: 2-D continuous wavelet transform for ESPI phase-maps denoising. Opt. Lasers Eng. **51**(9), 1060–1065 (2013)
19. Servin, M., Rodriguez-Vera, R., Marroquin, J., Malacara, D.: Phase-shifting interferometry using a two-dimensional regularized phase-tracking technique. J. Mod. Opt. **45**(9), 1809–1819 (1998)
20. Servin, M., Cuevas, F.J., Malacara, D., Marroquin, J.L., Rodriguez-Vera, R.: Phase unwrapping through demodulation by use of the regularized phase-tracking technique. Appl. Opt. **38**(10), 1934–1941 (1999)
21. Villa, J., Servin, M.: Robust profilometer for the measurement of 3-d object shapes based on a regularized phase tracker. Opt. Lasers Eng. **31**(4), 279–288 (1999)
22. Rivera, M.: Robust phase demodulation of interferograms with open or closed fringes. JOSA A **22**(6), 1170–1175 (2005)
23. Marroquin, J., Servin, M., Rodriguez-Vera, R.: Adaptive quadrature filters and the recovery of phase from fringe pattern images. JOSA A **14**(8), 1742–1753 (1997)
24. Kemao, Q., Soon, S.H.: Sequential demodulation of a single fringe pattern guided by local frequencies. Opt. Lett. **32**(2), 127–129 (2007)
25. Wang, H., Kemao, Q.: Frequency guided methods for demodulation of a single fringe pattern. Opt. Express **17**(17), 15118–15127 (2009)
26. Kai, L., Kemao, Q.: Fast frequency-guided sequential demodulation of a single fringe pattern. Opt. Lett. **35**(22), 3718–3720 (2010)
27. Dalmau-Cedeño, O.S., Rivera, M., Legarda-Saenz, R.: Fast phase recovery from a single closed-fringe pattern. JOSA A **25**(6), 1361–1370 (2008)
28. Deepan, B., Quan, C., Tay, C.: A derivative based simplified phase tracker for a single fringe pattern demodulation. Opt. Lasers Eng. **83**, 83–89 (2016)
29. Antoine, J.-P., Murenzi, R., Vandergheynst, P., Ali, S.T.: Two-dimensional wavelets and their relatives. Am. Math. Soc. **43**, 269–272 (2008)
30. Ma, J., Wang, Z., Pan, B., Hoang, T., Vo, M., Luu, L.: Two-dimensional continuous wavelet transform for phase determination of complex interferograms. Appl. Opt. **50**(16), 2425–2430 (2011)
31. Kulkarni, R., Rastogi, P.: Simultaneous estimation of unwrapped phase and phase derivative from a closed fringe pattern. Opt. Lasers Eng. **87**, 168–175 (2016)
32. Gdeisat, M.A., Burton, D.R., Lalor, M.J.: Spatial carrier fringe pattern demodulation by use of a two-dimensional continuous wavelet transform. Appl. Opt. **45**(34), 8722–8732 (2006)